

Article

Solid-State Luminescence with a Large Stokes Shift in Starch Functionalized with Low-Content ESIPT Dye

Emerson Colonetti , Lilian C. da Luz and Fabiano S. Rodembusch * 

Laboratory of Molecular Catalysis (LAMOCA), Instituto de Química, Universidade Federal do Rio Grande do Sul (UFRGS), P.O. Box 15003, Porto Alegre 91501-970, RS, Brazil; colonettiemerson@hotmail.com (E.C.); lilian.luz@ufrgs.br (L.C.d.L.)

* Correspondence: fabiano.rodembusch@ufrgs.br

Abstract: Herein, we present the preparation of solid-state photoactive starches with a large Stokes shift, along with the resulting materials. In this investigation, 2-(2'-hydroxyphenyl)benzazole derivatives responsive to intramolecular proton transfer in the excited state (ESIPT) were covalently bonded to the polymeric structure of starch through a reaction involving an isothiocyanate group and the hydroxyl groups of starch. These compounds exhibit absorption at approximately 350 nm, which is related to fully spin- and symmetry-allowed $\pi \rightarrow \pi^*$ electronic transitions, and solid-state fluorescence at approximately 500 nm, which features a significant separation between the absorption and emission maxima ($\sim 9000 \text{ cm}^{-1}$). Due to the minimal use of fluorophores in functionalized starch preparation, this modification does not affect the original properties of the starch. Finally, photoactive starch-based films with significantly high transparency were successfully produced.

Keywords: photoactive starch; ESIPT; large Stokes shift; biodegradable polymer; tagging material

1. Introduction

Plastics have become ingrained in daily routines, as they find applications across various industries [1]. Originating from synthetic polymers derived from nonrenewable petroleum sources, these materials present environmental challenges due to their resistance to degradation and prolonged persistence in the environment [2]. As concerns about their environmental impact intensify, there is growing interest in alternative materials that can replace traditional polymers. In response to these concerns, biopolymers are emerging as promising substitutes, primarily sourced from renewable raw materials and often exhibiting biodegradable properties [3–5]. Starch, an abundantly available natural resource, serves as a cost-effective renewable raw material for biopolymer production [6–10]. The conversion of starch into a thermoplastic polymer, known as thermoplastic starch (TPS), is facilitated through the incorporation of plasticizers [11,12]. Plasticizers, such as glycerol, sorbitol, glycols, and urea, enable the processing of TPS by reducing intermolecular hydrogen bonds within starch grains. The type and proportion of plasticizer used significantly impact the physical properties of the processed TPS, including the glass transition temperature and mechanical characteristics. Due to its hydrophilic nature, TPS is highly susceptible to moisture absorption, which affects its mechanical properties. Efforts to alleviate this sensitivity involve blending TPS with other materials to enhance its final properties and reduce vulnerability to environmental factors such as humidity, temperature, and radiation exposure [13–16].

Starch can undergo functionalization by introducing chemical groups through hydroxyl groups, significantly broadening the range of applications for the resulting material [17–19]. This expansion is not limited to the acquisition of thermoplastic materials. In the literature, light-emitting groups are attached to polysaccharide skeletons, demonstrating diverse applications [20–23]. However, there are currently few reports on the functionalization of starch with fluorescent compounds using excited-state intramolecular



Citation: Colonetti, E.; da Luz, L.C.; Rodembusch, F.S. Solid-State Luminescence with a Large Stokes Shift in Starch Functionalized with Low-Content ESIPT Dye. *Colorants* **2024**, *3*, 99–110. <https://doi.org/10.3390/colorants3020007>

Academic Editor: Anthony Harriman

Received: 19 December 2023

Revised: 15 February 2024

Accepted: 29 March 2024

Published: 3 April 2024



Copyright: © 2024 by the authors. Licensee MDPI, Basel, Switzerland. This article is an open access article distributed under the terms and conditions of the Creative Commons Attribution (CC BY) license (<https://creativecommons.org/licenses/by/4.0/>).

proton transfer (ESIPT), usually related to advancing methods for detecting and visualizing latent fingerprints, with improvements in sensitivity, selectivity, and ease of visualization on diverse substrates [24,25].

In 1955, Weller discovered the excited-state intramolecular proton transfer (ESIPT) process in salicylic acid, which exhibited a remarkable Stokes shift compared to that of analogs [26]. ESIPT-active fluorophores, known for their photophysical stability and large Stokes shift (6000 to $12,000$ cm^{-1}), have become a focal point in research [27–30]. These compounds, which have dual fluorescence emission and sensitivity to the environment, have diverse applications [31–42]. ESIPT in benzazole derivatives relies on factors such as intramolecular hydrogen bonds, electronic effects of donor ($-\text{OH}$) and acceptor ($-\text{C}=\text{N}-$) groups, and molecular geometry. The delicate balance between structural and electronic aspects determines the occurrence of ESIPT, which is essential for its successful execution [31]. Benzazole heterocycles, aromatic compounds with a benzene-azole ring fusion, play a crucial role in heterocyclic compounds, forming benzoxazoles, benzimidazoles, benzothiazoles, or benzoselenazoles [43]. These compounds, which contain diverse heteroatoms, are fundamental building blocks in medicinal chemistry for synthesizing biologically active molecules [44–47] and photoactive polymeric materials [48–53]. Regarding ESIPT and benzazoles, hydroxyphenylbenzazoles, which can undergo proton transfer in the excited state, exist predominantly as enol (E) species in the ground state (Figure 1) [28]. Upon excitation, a redistribution of charges leads to intramolecular proton transfer, giving rise to a new keto tautomer and fluorescence emission with a large Stokes shift. In addition, these fluorophores can also exhibit dual fluorescence emission, with distinct bands corresponding to additional enol conformers (blue line) and keto tautomers (red line) influenced by the surrounding medium [54].

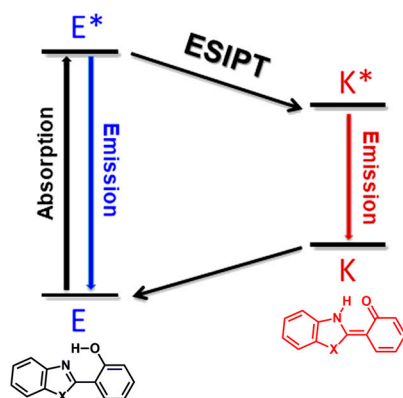


Figure 1. The ESIPT process, where E and K denote the enol conformer and keto tautomer, respectively, and the asterisk indicates the excited state.

In this context, our investigation focused on creating fluorescent starches by introducing excited-state intramolecular proton transfer (ESIPT) dyes through starch functionalization. The objective of this study was to incorporate the inherent photophysical properties of the ESIPT process, such as solid-state emission, fluorescence with a large Stokes shift, and photostability, into starch matrices. The ultimate aim is to produce novel biocompatible and biodegradable fluorescent materials. The development of these new materials is crucial for merging the advantages of fluorescence with environmentally friendly attributes. These materials have diverse applications, ranging from environmental monitoring to medical imaging, aligning with the increasing demand for sustainable and eco-friendly solutions. For this purpose, benzazoles functionalized with isothiocyanate will be used to covalently attach these fluorophores to starch, forming a thiocarbamate bond. The resulting functionalized starches will be employed in the fabrication of solid-state photoactive thermoplastic films.

2. Experimental Section

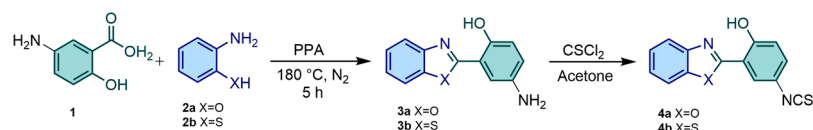
2.1. Materials and Methods

Natural corn starch (Amisol 3408, Ingredion Brasil Ing. Ind. Ltda, Mogi Guaçu, SP, Brazil) was used as received. Commercially available reagents and solvents (acetone, dichloromethane, dimethylsulfoxide, methanol, glycerin, and distilled water) were used as received without additional purification. Thin-layer chromatography (TLC) was performed using the supported silica gel GF254 (0.25 mm thickness). For visualization, TLC plates were placed under UV light at 254 nm. X-ray diffraction analyses were performed on a diffractometer (Shimadzu XRD 6000, Shimadzu, Kyoto, Japan) with $k\text{-}\alpha$ radiation and a wavelength of 1.5406 Å. The reading range was from 4 to 45° with a step of 2° min⁻¹. Thermogravimetric analysis (TGA) of the photoactive starches and respective thermoplastic films was conducted using a Shimadzu TGA-50 (Shimadzu) thermogravimetric analyzer under a nitrogen atmosphere with a flow rate of 50 mL·min⁻¹ and a heating rate of 10 °C·min⁻¹. Fourier transform infrared (FT-IR) spectra were recorded on a Shimadzu IR Prestige-21 (Shimadzu) spectrometer in the range of 400–4000 cm⁻¹ with a spectral resolution of 4 cm⁻¹ using KBr pellets. UV–Vis absorption spectra were obtained using a Shimadzu UV2450PC (Shimadzu) spectrophotometer. All the experiments were conducted at room temperature (25 °C) for both the powder and film samples. Solid-state measurements utilized an ISR2200 integrating sphere. Barium sulfate (BaSO₄) (Wako Pure Chemical Industries, Ltd., Tokyo, Japan) was used for the experiments at room temperature. Fluorescence emission spectra were obtained using a Shimadzu RF5301PC (Shimadzu) spectrofluorometer. All the experiments were conducted at room temperature (25 °C) for both the powder and film samples. The wavelength of the maximum UV–Vis absorption band was used as the excitation wavelength for fluorescence emission measurements. For solid-state samples, support was used where the angle of incidence of radiation was 45° relative to the detector. The solid-state relative fluorescence quantum yields were determined by employing sodium salicylate as the standard ($QY_{SS} = 0.55$) [55,56]. This involved a comparison of the integrated area of the emission spectrum of the benzazole derivatives (A_{BZ}) with that of sodium salicylate (A_{SS}). The percentage reflectance of the benzazole (R_{BZ}) and the reference sodium salicylate (R_{SS}) was measured relative to a plate coated with barium sulfate at the wavelength of maximum excitation. The fluorescence quantum yield of the benzazoles (QY_{BZ}) was calculated using Equation (1), where $\Phi_{FL ss}$ represents the fluorescence quantum yield of the reference material. In this experiment, the samples were treated as powders.

$$QY_{SS} = QY_{BZ} \frac{A_{BZ} 100 - R_{SS}}{A_{SS} 100 - R_{BZ}} \quad (1)$$

2.2. Synthesis

The studied 2-(2'-hydroxyphenyl)benzazole derivatives **4a–4b** were prepared as described in the literature [57,58]. In general, the respective amino precursors 2-(5'-amino-2'-hydroxyphenyl)benzazoles **3a–3b** were prepared from the condensation of 5-aminosalicylic acid (**1**) with *o*-substituted anilines **2a** or **2b** in polyphosphoric acid, resulting in the formation of the corresponding aminobenzazoles **3a–3b** [59]. For purification, chromatography in a column was performed on silica gel (230–400 mesh) using dichloromethane as the eluent. To obtain isothiocyanate derivatives **4a–4b** (Scheme 1), a solution of **3a** (or **3b**) in dry acetone was slowly added dropwise to a solution of thiophosgene (Cl₂CS) in dry acetone (1:5) at 0 °C. The reaction mixture was stirred for two hours at room temperature, leading to the formation of the desired products. The resulting precipitate was filtered, washed with cold acetone, and subsequently dried at 60 °C. Purification was accomplished through chromatography in a column on silica gel (230–400 mesh) using dichloromethane as the eluent. The spectroscopic characterization aligns with the literature and conforms to the anticipated chemical structures.



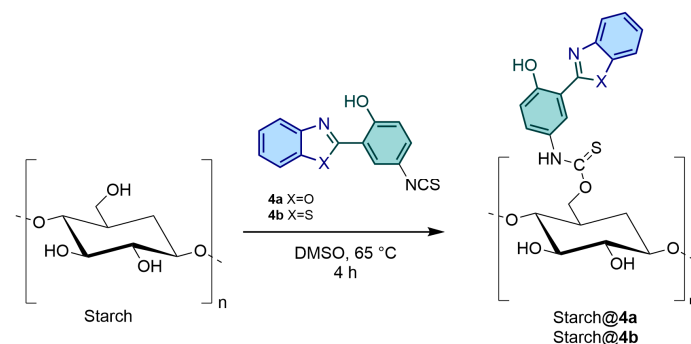
Scheme 1. Synthetic route for obtention of isothiocyanate derivatives **4a–4b**.

2-(5'-Isothiocyanate-2'-hydroxyphenyl)benzoxazole (**4a**). Yield: 90%. M.p.: 169–171 °C. $^1\text{H NMR}$ (400 MHz, CDCl_3) δ (ppm): 11.62 (s, 1H), 7.08 (dd, 1H, $J = 8.8$ Hz), 7.88 (d, 1H, $J = 2.4$ Hz), 7.74 (m, 1H), 7.62 (m, 1H), 7.42 (m, 2H), 7.42 (m, 2H), 7.28 (dd, 1H, $J = 9.2, 2.8$ Hz). FTIR (wavenumber, cm^{-1}): 3062, 2100, 1629, 1488, 1231.

2-(5'-Isothiocyanate-2'-hydroxyphenyl)benzothiazole (**4b**). Yield: 92%. M.p.: 152–157 °C. $^1\text{H NMR}$ (400 MHz, CDCl_3) δ (ppm): 12.74 (s, 1H), 7.99 (m, 1H), 7.92 (m, 1H), 7.53 (m, 2H), 7.45 (m, 1H), 7.24 (dd, 1H, $J = 8.8, 2.4$ Hz), 7.06 (d, 1H, $J = 8.8$ Hz). FTIR (wavenumber, cm^{-1}): 3022, 2101, 1585, 1483, 1263.

2.3. Preparation of Fluorescent Starch

The general procedure used to prepare the fluorescent starch is presented in Scheme 2. An amount of 2 g of pure starch was dissolved in 50 mL of DMSO at 65 °C for 30 min. Subsequently, different amounts of fluorophore **4a** or **4b** were introduced into the reaction system, and the mixture was stirred at 65 °C for an additional 4 h. During this phase, we conducted reactions using different amounts of fluorophores to starch (w/w), as outlined in Table 1. The aim was to evaluate the properties of the resulting materials concerning fluorophore concentration. After this period, the solution was allowed to cool to room temperature (25 °C). Following the completion of the reaction, 150 mL of methanol was added to this solution. The resulting precipitate was then filtered and washed with methanol (3×20 mL) and acetone (3×20 mL) to remove the unbound fluorophore. The resultant precipitate was air-dried for 24 h at room temperature (25 °C) and for an additional 24 h at 65 °C under vacuum. Finally, the dried precipitate was comminuted in a mortar for characterization purposes.



Scheme 2. Synthetic route for obtention fluorescent starches.

Table 1. Reaction conditions for the preparation of modified starches.

Fluorophore	Starch (g)	Fluorophore Amount (w%) ¹	Nomenclature
4a	2.0	0.1	Starch@ 4a 01
		0.5	Starch@ 4a 05
		1.0	Starch@ 4a 1
		5.0	Starch@ 4a 5
4b	2.0	0.1	Starch@ 4b 01
		0.5	Starch@ 4b 05
		1.0	Starch@ 4b 1
		5.0	Starch@ 4b 5

¹ Derived from the initial amount of starch employed in the calculation.

2.4. Fluorescent Films Based on Starch

The casting technique was employed to prepare fluorescent starch films with glycerol as the plasticizer in different proportions (Table 2). Natural corn starch (used as a blank sample) or fluorescent starch (Starch@4a5 or Starch@4b5) was dissolved in deionized water at 75 °C under mechanical stirring for 1 h. Glycerol was then introduced into the starch solution, and the mixture was stirred for an additional 15 min. Notably, at this stage, starch films were also produced through simple mixing, wherein fluorophores, without covalent bonding to starch, were added during the dissolution of starch. This step served as a control for evaluating the resulting fluorescent materials. The resulting solutions or mixtures were poured into polypropylene Petri dishes and dried in an oven at 65 °C for 24 h.

Table 2. Reaction conditions for the preparation of fluorescent films based on modified starch.

Component	Amount (w%) ¹		
	Film Starch	Film Starch@4a	Film Starch@4b
Starch	70	-	-
Glycerol	30	30	30
Starch@4a5	-	70	-
Starch@4b5	-	-	70

¹ Derived from the initial amount of starch employed in the calculation.

3. Results and Discussion

3.1. Characterization

The characterization of photoactive-doped materials heavily relies on the concentration of fluorophores, and various techniques can be employed to clarify binding, each operating at different sensitivities. However, the literature notes the intricacy of this characterization when a low content of fluorophores is utilized [60,61], which is precisely the situation with the modified starches prepared in this study. The morphology of the modified starches was first investigated using X-ray diffraction (XRD) (Figure 2). Substituting hydroxyl groups in starch can cause alterations in its crystalline structure. For example, when acetylation occurs on starch, a new X-ray diffraction pattern is generated, providing a means to evaluate the effectiveness of these reactions [62–64]. The diffraction pattern of natural starch displays peaks at approximately 15°, 16°, 17°, and 23° (2θ), as expected for corn starch [64,65]. X-ray diffraction analyses thus indicate a departure from the usual crystalline structure observed in natural starch when examining photoactive starches. The literature highlights that the processing of starch can induce significant structural alterations. A widely employed processing step is gelatinization, which involves the heating of starch in excess water within the temperature range of 50 to 70 °C. Throughout this procedure, a cooperative transition occurs wherein water infiltrates the amorphous regions of the granules, resulting in their swelling and destabilization of the crystalline regions. Consequently, this induces rapid granule swelling, crystallite melting, and complete loss of ordered structure [66–68]. Because starch modification occurs at 65 °C in the presence of undried DMSO, the loss of crystallinity could be related to the gelatinization process. Furthermore, due to the low water content, the efficiency of the process was not absolute, allowing for the discernment of some degree of ordered structure. In addition, despite the limited presence of fluorophores in starch reactions, which leads to minimal substitution of starch hydroxyl groups, the influence of fluorophores on the loss of crystallinity observed in modified starches compared to pure starch cannot be ruled out. With respect to the substitution of starch hydroxyl groups, each repeating unit of α-D-glucopyranose in starch has three hydroxyl groups available for reactions. The literature suggests a maximum possible degree of substitution of 3.0 [69]. For instance, the calculated degree of substitution for the highest concentration (5%) of 2-(5'-isothiocyanato-2'-hydroxyphenyl)benzoxazole (4b), assuming 100% reaction with starch, would be 0.06. Consequently, only approximately 2% of the hydroxyl groups in the α-D-glucopyranose units would undergo substitution.

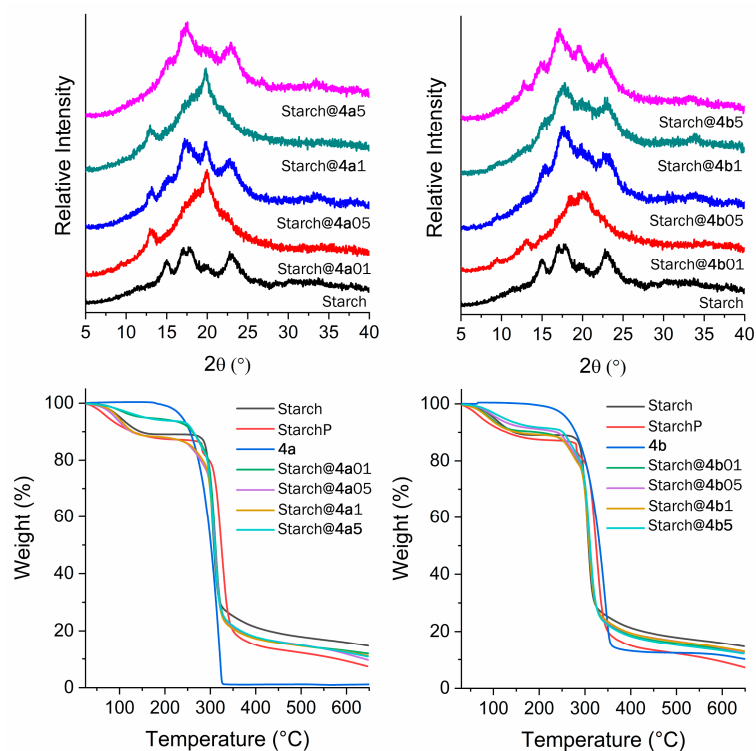


Figure 2. Modified starch characterization prepared using fluorophore **4a** (left) and **4b** (right), where (top) XRD and (bottom) TGA thermograms.

According to the thermogravimetric analyses, presented in Figure 2 (bottom), the modified starch exhibited behavior reminiscent of that of natural starch, revealing two distinct stages below 500 °C. Note that an additional sample was prepared for comparison, the so-called StarchP. This sample was processed in the same manner as the modified starches but without the addition of a fluorophore. The initial stage, marked by a slight mass loss just above 100 °C, is linked to water loss, while the second stage, occurring at approximately 300 °C with substantial mass loss, corresponds to polymer decomposition. Both the starch and modified starch samples undergo a mass loss of approximately 15% up to nearly 100 °C, attributed to the absorption of water due to the hygroscopic nature of starch [64,70]. On the other hand, both fluorophores, **4a** and **4b**, demonstrate a single stage in their TGAs, indicating thermal degradation at approximately 300 °C. Finally, the infrared spectra presented in the Supplementary Material (Figures S4–S6) reveal strong absorption at approximately 2100 cm^{-1} for both studied fluorophores related to the $\text{N}=\text{C}=\text{S}$ bond vibrations. In addition, the localized absorptions at 1491 cm^{-1} and 1572 cm^{-1} (**4b**), as well as at 1507 cm^{-1} and 1586 cm^{-1} (**4a**), correspond to aromatic $\text{C}=\text{C}$ bond vibrations. A specific absorption at 1445 cm^{-1} ($\text{C}=\text{C}$ aromatic stretching) was observed, along with absorptions at 1653 cm^{-1} (carbonyl $\text{C}=\text{O}$) and 3500 cm^{-1} (medium intensity, stretching of the primary amine $\text{N}-\text{H}$ bond). In natural starch, localized absorptions at 1159, 1082, and 1014 cm^{-1} are related to $\text{C}-\text{O}$ stretching, while other bands at 992, 929, 861, 765, and 575 cm^{-1} are due to stretching vibrations of the anhydroglucose unit [62,63]. Similar results were observed for processed starch (StarchP). The broad band at 3425 cm^{-1} is attributed to hydroxyl groups, and at 1641 cm^{-1} , strongly bound water is observed [62,63]. Notably, no infrared absorption related to the fluorophores was detected in the modified starches. The anticipated band at approximately 1550 cm^{-1} ($\text{NH}(\text{C}=\text{S})$ group) is absent, which should result from the formation of a thiocarbamate group during the reaction between $-\text{OH}$ and isothiocyanate. Additionally, the characteristic band of $\text{N}=\text{C}=\text{S}$ bond vibrations in unreacted fluorophores was not observed, possibly due to the low fluorophore content used in the starch reactions. Detecting very small quantities or dilutions in the polymer chain is challenging with FTIR [71].

3.2. Photophysics

The obtained modified starches were characterized in the solid state using UV–Vis absorption and fluorescence emission spectroscopies. The relevant data are summarized in Table 3. All the experiments were performed under the same conditions, using 50 mg of each sample, which was treated as powder. Each modified starch sample exhibited a distinct absorption in the visible region, which intensified at higher energies, below 400 nm (Figure 3a,b). Furthermore, there is an increase in absorption at approximately 350 nm as the concentration of fluorophores increases during starch preparation, which could be related to the absorption of the fluorophore. It is also noteworthy that with an elevated fluorophore concentration, the absorption maxima shifts toward the corresponding maxima observed for pure fluorophores (Figure 3c). Finally, it was observed that the pure starch in the solid state (blank sample) presented absorption below 300 nm, as already reported in the literature [72,73].

Table 3. Photophysical data in the solid state for modified starches using fluorophores **4a** and **4b**, where λ_{abs} and λ_{em} are the absorption and emission maxima, respectively, $\Delta\lambda_{\text{ST}}$ is the Stokes shift, and QY is the fluorescence quantum yield.

Sample	λ_{abs}	λ_{em}	$\Delta\lambda_{\text{ST}}$ (nm/cm ⁻¹)	QY (%)
Starch@4a01	333	514	181/10575	1.1
Starch@4a05	344	512	168/9539	3.4
Starch@4a1	350	511	161/9002	4.5
Starch@4a5	366	512	146/7791	7.6
Starch@4b01	334	501	167/9980	1.8
Starch@4b05	345	503	158/9105	3.3
Starch@4b1	366	503	137/7442	4.2
Starch@4b5	362	540	178/9106	1.1

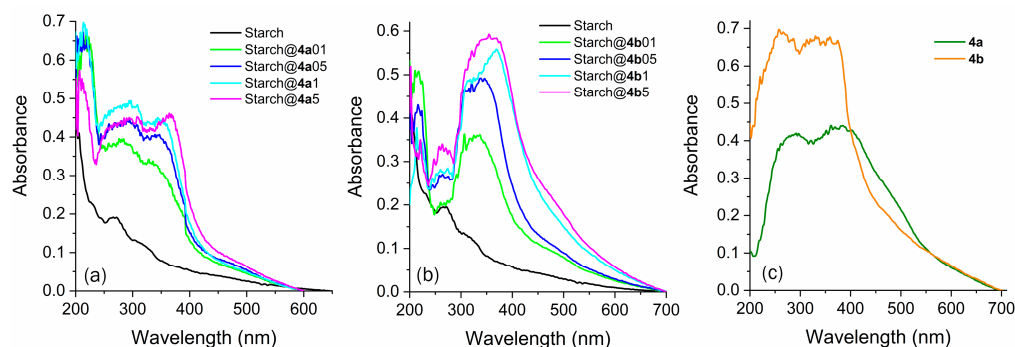


Figure 3. Absorption spectra in the solid-state (DRUV) of the obtained modified starches prepared with different fluorophore amounts using (a) **4a** and (b) **4b**. (c) DRUV spectra of pure fluorophores are presented for comparison.

In Figure 4a,b, the emission curves of the modified starches are depicted, clearly indicating that all the samples exhibited photoactivity within the 450–650 nm range. Unlike what was noted in absorption, the emission spectra show notable distinctions when the fluorophores are bound to starch, suggesting that the matrix influences the photophysical properties of these compounds. The emission peaks for modified starches prepared with fluorophore **4a** are situated at approximately 510 nm (Figure 4a), matching the region observed for the pure fluorophore (Figure 4c). Specifically, the resemblance between the spectra of the pure fluorophore and modified starch samples suggested that the photophysical behavior of **4a** was similar, regardless of whether it was covalently linked to the polymer chain of starch. In addition, in the modified starches prepared with fluorophore **4a**, there was an increase in the emission intensity of the photoactive starch as the quantity of fluorophore used for the preparation of the materials increased, in accordance with expectations. However, modified

starches prepared using **4b** as a fluorophore exhibited different photophysical behaviors. Initially, after binding with starch, the emission maxima of fluorophore **4b** shifted toward blue (500 nm) compared with that of the pure fluorophore (530 nm). This behavior has already been observed when benzazoles reactive to the ESPT mechanism are covalently attached or doped into organic or inorganic matrices, highlighting the sensitivity of these fluorophores to the environment [74,75]. Additionally, as observed for starch doped with fluorophore **4a**, samples prepared with **4b** showed that the emission intensity was dependent on the dye concentration in the starch (from Starch@**4b**01 to Starch@**4b**1). Additionally, the modified starch prepared with more fluorophore (Starch@**4b**5) exhibited an emission maximum located at 540 nm, which was less intense than that at lower concentrations. In this case, unlike what was noted in absorption, the emission spectra show notable distinctions when the fluorophores are bound to starch, suggesting an additional nonradiative energy loss in the excited state or even interaction with additional ES IPT dyes in the matrix. The pure starch did not exhibit fluorescence emission, as expected. Furthermore, regarding the Stokes shift, the calculated values are consistent with what is expected for the keto* emission arising from the ES IPT process, indicating the absence of dual emission or the favoring of conformers unresponsive to ES IPT. The low values for the fluorescence quantum yield were expected due to the low dye content and agree with similar structures presenting ES IPT, as reported in the literature [76]. Finally, we would like to emphasize that the correlation between the quantum yields in the solid state, emission curve profiles, and the location of their respective maxima suggests that the emitting species may be different. Although it is not possible to observe any red-shifted absorption band, corresponding to ionized species already present in the ground state, the literature reports that compounds that are reactive to ES IPT can ionize in the excited state, generating species with emissions distinct from those observed in their neutral analogs [76,77]. Although the Stokes shift values indicate the presence of keto emission, the possibility of ionization in the excited state should not be dismissed, since the remaining OH groups in the starch could serve as proton acceptors [77]. This property, stemming from these compounds' increased photoacidity, may contribute in some way to the distinct emissions observed.

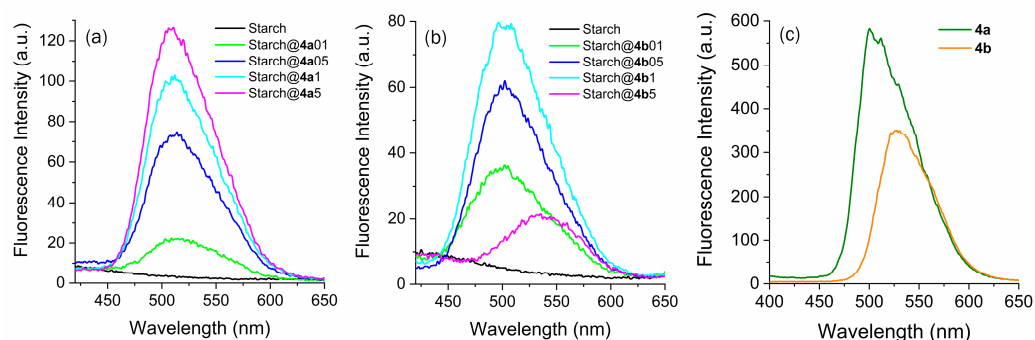


Figure 4. Steady-state emission spectra in the solid-state of the obtained modified starches prepared with different fluorophore amounts using (a) **4a** and (b) **4b**. (c) Solid-state emission spectra of pure fluorophores are presented for comparison.

As a proof of concept, films were prepared with modified starches, as shown in Figure 5. As noted in this study, the fluorophores exhibiting fluorescent properties were covalently bonded to the polymeric structure of starch through reactions with its hydroxyl groups. The quantity of compound used in modifying starch does not compromise its original properties, which allowed us to prepare these photoactive films. In this investigation, a control film (Figure 5a) prepared with nondoped starch was prepared for comparison (Table 2, Film Starch). The good transparency of the films prepared with pure starch and modified starches can be observed in Figure 5a–c. The films prepared with photoactive starches exhibited emission in the cyan-green to green regions, as expected from the emission results of the modified starches in the solid state.

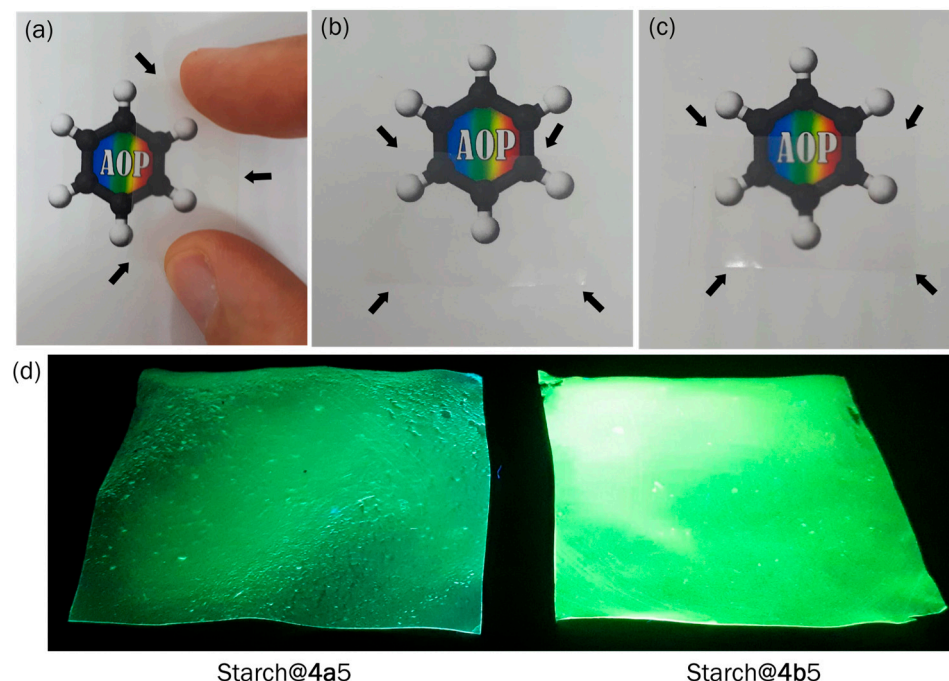


Figure 5. Photographs of the films prepared with (a) pure starch, (b) modified starch with **4a**, and (c) modified starch with **4b** under normal light. (d) Modified starch under UV light (365 nm). The black arrows indicate the boundaries of the starch films.

4. Conclusions

In this study, we successfully synthesized novel starch-based materials with solid-state fluorescence under mild reaction conditions. Thermal analyses revealed that the thermal behavior of natural starch remained largely unchanged after reactions with fluorophores. Although the X-ray diffraction patterns of the modified starches differed from those of natural starch, a consistent pattern was not observed. The presence of fluorophores in the starch polymeric matrix was confirmed through photophysical characterizations. The similarity between the spectra of pure fluorophores and modified starches, which feature a significant Stokes shift, suggests that the photophysical behavior of fluorophores is consistent, whether covalently linked to the polymeric chain of starch or not. Moreover, the modified starches developed in this study facilitated the creation of photoactive thermoplastic films.

Supplementary Materials: The following supporting information can be downloaded at: <https://www.mdpi.com/article/10.3390/colorants3020007/s1>, Figure S1: FTIR spectra of fluorophores **4a** and **4b**; Figure S2: ^1H NMR spectrum (CDCl_3 , 400 MHz) of fluorophore **4a**; Figure S3: ^1H NMR spectrum (CDCl_3 , 400 MHz) of fluorophore **4b**; Figure S4: FTIR spectra of starch and processed starch (StarchP); Figure S5: FTIR spectra of modified starches with fluorophore **4a**. StarchP spectrum was presented for comparison; Figure S6: FTIR spectra of modified starches with fluorophore **4b**. StarchP spectrum was presented for comparison.

Author Contributions: Conceptualization, F.S.R.; methodology, E.C.; validation, F.S.R.; formal analysis, E.C. and L.C.d.L.; resources, F.S.R.; writing—original draft preparation, F.S.R. and L.C.d.L.; writing—review and editing, F.S.R.; supervision, F.S.R.; project administration, F.S.R.; funding acquisition, F.S.R. All authors have read and agreed to the published version of the manuscript.

Funding: This research was funded by CNPq (305954/2019-9) and Coordenação de Aperfeiçoamento de Pessoal de Nível Superior-Brasil (CAPES)—Finance Code 001.

Institutional Review Board Statement: Not applicable.

Informed Consent Statement: Not applicable.

Data Availability Statement: Not applicable.

Conflicts of Interest: The authors declare no conflict of interest.

References

1. Geyer, R.; Jambeck, J.R.; Law, K.L. Production, use, and fate of all plastics ever made. *Sci. Adv.* **2017**, *3*, e1700782. [[CrossRef](#)] [[PubMed](#)]
2. Moshood, T.; Nawansir, G.; Mahmud, F.; Mohamad, F.; Ahmad, M.; AbdulGhani, A. Sustainability of biodegradable plastics: New problem or solution to solve the global plastic pollution? *Curr. Res. Green Sustain. Chem.* **2022**, *5*, 100273. [[CrossRef](#)]
3. Chen, G.; Patel, M. Plastics derived from biological sources: Present and Future: A technical and environmental review. *Chem. Rev.* **2012**, *112*, 2082–2099. [[CrossRef](#)] [[PubMed](#)]
4. Samir, A.; Ashour, F.; Hakim, A.; Bassyouni, M. Recent advances in biodegradable polymers for sustainable applications. *NPJ Mater. Degrad.* **2022**, *6*, 68. [[CrossRef](#)]
5. Rai, P.; Mehrotra, S.; Priya, S.; Gnansounou, E.; Sharma, S.K. Recent advances in the sustainable design and applications of biodegradable polymers. *Bioresour. Technol.* **2021**, *325*, 124739. [[CrossRef](#)] [[PubMed](#)]
6. Falua, K.; Pokharel, A.; Babaei-Ghazvin, A.; Ai, Y.; Acharya, B. Valorization of starch to biobased materials: A review. *Polymers* **2022**, *14*, 2215. [[CrossRef](#)] [[PubMed](#)]
7. Villwock, K.; BeMiller, J. The architecture, nature, and mystery of starch granules. Part 2. *Starch-Stärke* **2022**, *74*, 2100184. [[CrossRef](#)]
8. Pérez, S.; Bertoft, E. The molecular structures of starch components and their contribution to the architecture of starch granules: A comprehensive review. *Starch-Stärke* **2010**, *62*, 389–420. [[CrossRef](#)]
9. Xu, H.; Zhou, J.; Liu, X.; Yu, J.; Copeland, L.; Wang, S. Methods for characterizing the structure of starch in relation to its applications: A comprehensive review. *Crit. Rev. Food Sci. Nutr.* **2023**, *63*, 4799–4816. [[CrossRef](#)]
10. Nafchi, A.; Moradpour, M.; Saeidi, M.; Alias, A. Thermoplastic starches: Properties, challenges, and prospects. *Starch-Stärke* **2013**, *65*, 61–72. [[CrossRef](#)]
11. Bangar, S.; Whiteside, W.; Ashogbon, A.; Kumar, M. Recent advances in thermoplastic starches for food packaging: A review. *Food Packag. Shelf Life* **2021**, *30*, 100743. [[CrossRef](#)]
12. Chen, Y.; Shull, K. Controlling the properties of thermoplastic starch films with hydrogen bonding plasticizers. *Carbohydr. Polym. Technol. Appl.* **2023**, *5*, 100291. [[CrossRef](#)]
13. Montilla-Buitrag, C.; Gómez-López, R.; Solanilla-Duque, J.; Serna-Cock, L.; Villada-Castill, H. Effect of plasticizers on properties, retrogradation, and processing of extrusion obtained thermoplastic starch: A review. *Starch-Stärke* **2021**, *73*, 2100060. [[CrossRef](#)]
14. Yang, J.; Wang, Z.; Ren, J.; Lin, X.; Zhao, J.; Jiang, X.; Chen, Y. Molecular dynamics simulation and properties of thermoplastic starch-effect of water content on starch plasticization. *Polymer* **2024**, *290*, 126571. [[CrossRef](#)]
15. Leroy, L.; Stoclet, G.; Lefebvre, J.; Gaucher, V. Mechanical behavior of thermoplastic starch: Rationale for the temperature-relative humidity equivalence. *Polymers* **2022**, *14*, 253. [[CrossRef](#)] [[PubMed](#)]
16. Diyana, Z.; Jumaidin, R.; Selamat, M.; Ghazali, I.; Julmohammad, N.; Huda, N.; Ilyas, R. Physical properties of thermoplastic starch derived from natural resources and its blends: A review. *Polymers* **2021**, *13*, 1396. [[CrossRef](#)] [[PubMed](#)]
17. Surendren, A.; Mohanty, A.; Liu, Q.; Misra, M. A review of biodegradable thermoplastic starches, their blends and composites: Recent developments and opportunities for single-use plastic packaging alternatives. *Green. Chem.* **2022**, *24*, 8606–8636. [[CrossRef](#)]
18. Bulatović, V.; Mandić, V.; Grgić, D.; Ivančić, A. Biodegradable polymer blends based on thermoplastic starch. *J. Polym. Environ.* **2021**, *29*, 492–508. [[CrossRef](#)]
19. Li, Y.; Tan, Y.; Ning, Z.; Sun, S.; Gao, Y.; Wang, P. Design and fabrication of fluorescein-labeled starch-based nanospheres. *Carbohydr. Polym.* **2011**, *86*, 291–295. [[CrossRef](#)]
20. Li, H.; Guo, X.; Liu, J.; Li, F. A synthesis of fluorescent starch based on carbon nanoparticles for fingerprints detection. *Opt. Mater.* **2016**, *50*, 404–410. [[CrossRef](#)]
21. Li, H.; Zhang, B.; Lü, S.; Ma, H.; Liu, M. Synthesis and characterization of a nano fluorescent starch. *Int. J. Biol. Macromol.* **2018**, *120*, 1225–1231. [[CrossRef](#)]
22. Cai, C.; Wei, B.; Jin, Z.; Tian, Y. Facile method for fluorescent labeling of starch nanocrystal. *ACS Sustain. Chem. Eng.* **2017**, *5*, 3751–3761. [[CrossRef](#)]
23. Javanbakht, S.; Namazi, H. Solid state photoluminescence thermoplastic starch film containing graphene quantum dots. *Carbohydr. Polym.* **2017**, *176*, 220–226. [[CrossRef](#)] [[PubMed](#)]
24. Barros, H.L.; Stefani, V. Synthesis and photophysical behavior of fluorescent benzazole dyes and fluorescent microparticles: Their use as fingerprint developer. *J. Photochem. Photobiol. A Chem.* **2021**, *420*, 113494. [[CrossRef](#)]
25. Barros, H.L.; Tavares, L.; Stefani, V. Dye-doped starch microparticles as a novel fluorescent agent for the visualization of latent fingerprints on porous and non-porous substrates. *Forensic Chem.* **2020**, *20*, 100264. [[CrossRef](#)]
26. Weller, A. Über die fluoreszenz der salizylsäure und verwandter verbindungen. *Sci. Nat.* **1955**, *42*, 175–176. [[CrossRef](#)]
27. Kwon, J.E.; Park, S.Y. Advanced organic optoelectronic materials: Harnessing excited-state intramolecular proton transfer (ESIPT) process. *Adv. Mater.* **2011**, *23*, 3615–3642. [[CrossRef](#)] [[PubMed](#)]
28. Li, Y.; Dahal, D.; Abeywickrama, C.S.; Pang, Y. Progress in tuning emission of the excited-state intramolecular proton transfer (ESIPT)-based fluorescent probes. *ACS Omega* **2021**, *6*, 6547–6553. [[CrossRef](#)] [[PubMed](#)]

29. Padalkar, V.S.; Seki, S. Excited-state intramolecular proton-transfer (ESIPT)-inspired solid state emitters. *Chem. Soc. Rev.* **2015**, *45*, 169–202. [[CrossRef](#)]
30. Santos, F.S.; Ramasamy, E.; Ramamurthy, V.; Rodembusch, F.S. Excited state behaviour of benzoxazole derivatives in a confined environment afforded by a water soluble octaacid capsule. *J. Photochem. Photobiol. A Chem.* **2016**, *317*, 175–185. [[CrossRef](#)]
31. Zhao, J.; Ji, S.; Chen, Y.; Guo, H.; Yang, P. Excited state intramolecular proton transfer (ESIPT): From principal photophysics to the development of new chromophores and applications in fluorescent molecular probes and luminescent materials. *Phys. Chem. Chem. Phys.* **2012**, *14*, 8803–8817. [[CrossRef](#)]
32. Sedgwick, A.C.; Wu, L.; Han, H.H.; Bull, S.D.; He, X.P.; James, T.D.; Sessler, J.L.; Tang, B.Z.; Tian, H.; Yoon, J. Excited-state intramolecular proton-transfer (ESIPT) based fluorescence sensors and imaging agents. *Chem. Soc. Rev.* **2018**, *47*, 8842–8880. [[CrossRef](#)] [[PubMed](#)]
33. Nehra, N.; Kaushik, R. ESIPT-based probes for cations, anions and neutral species: Recent progress, multidisciplinary applications and future perspectives. *Anal. Methods* **2023**, *15*, 5268–5285. [[CrossRef](#)] [[PubMed](#)]
34. Wu, Y.; Wang, R.; Lin, R.; Xu, X.; Zhang, X.; Alsaman, O.; Qiu, Y.; Uddin, A.; Ouyang, X. Excited-state intramolecular proton transfer emitter for efficient violet-blue organic light-emitting diodes with hybridized local/charge transfer channel. *Chem. Eng. J.* **2023**, *465*, 142929. [[CrossRef](#)]
35. Trannoy, V.; Léaustic, A.; Gadan, S.; Guillot, R.; Allain, C.; Clavier, G.; Mazerat, S.; Geffroy, B.; Yu, P. A highly efficient solution and solid state ESIPT fluorophore and its OLED application. *New J. Chem.* **2021**, *45*, 3014–3022. [[CrossRef](#)]
36. Singh, A.K.; Nair, A.V.; Shah, S.S.; Ray, S.; Singh, N.D.P. ESIPT-, AIE-, and AIE + ESIPT-based light-activated drug delivery systems and bioactive donors for targeted disease treatment. *J. Med. Chem.* **2023**, *66*, 3732–3745. [[CrossRef](#)]
37. Bhosle, A.A.; Banerjee, M.; Barooah, N.; Bhasikuttan, A.C.; Kadu, K.; Ramanan, S.R.; Chatterjee, A. ESIPT-active hydroxybenzothiazole-picolinium@CB[7]-HAp NPs based supramolecular sensing assembly for spermine, spermidine and cadaverine: Application in monitoring cancer biomarkers and food spoilage. *J. Photochem. Photobiol. A Chem.* **2022**, *426*, 113770. [[CrossRef](#)]
38. Wang, Y.; Zhu, M.; Jiang, E.; Hua, R.; Na, R.; Li, Q.X. A Simple and rapid turn on ESIPT fluorescent probe for colorimetric and ratiometric detection of biothiols in living cells. *Sci. Rep.* **2017**, *7*, 4377. [[CrossRef](#)] [[PubMed](#)]
39. Mamada, M.; Inada, K.; Komino, T.; Potscavage, W.J., Jr.; Nakanotani, H.; Adachi, C. Highly efficient thermally activated delayed fluorescence from an excited-state intramolecular proton transfer system. *ACS Cent. Sci.* **2017**, *3*, 769–777. [[CrossRef](#)]
40. Gu, H.; Wang, W.; Wu, W.; Wang, M.; Liu, Y.; Jiao, Y.; Wang, F.; Wang, F.; Chen, X. Excited-state intramolecular proton transfer (ESIPT)-based fluorescent probes for biomarker detection: Design, mechanism, and application. *Chem. Commun.* **2023**, *59*, 2056–2071. [[CrossRef](#)]
41. Li, J.; Wu, Y.; Xu, Z.; Liao, Q.; Zhang, H.; Zhang, Y.; Xiao, L.; Yao, J.; Fu, H. Tuning the organic microcrystal laser wavelength of ESIPT-active compounds via controlling the excited enol* and keto* emissions. *J. Mater. Chem. C* **2017**, *5*, 12235–12240. [[CrossRef](#)]
42. Guo, L.; Tian, M.; Zhang, Z.; Lu, Q.; Liu, Z.; Niu, G.; Yu, X. Simultaneous two-color visualization of lipid droplets and endoplasmic reticulum and their interplay by single fluorescent probes in lambda mode. *J. Am. Chem. Soc.* **2021**, *143*, 3169–3179. [[CrossRef](#)] [[PubMed](#)]
43. Lokwani, P.; Nagori, B.P.; Batra, N.; Goyal, A.; Gupta, S.; Singh, N. Benzoxazole: The molecule of diverse biological activities. *J. Chem. Pharm. Res.* **2011**, *3*, 302–311.
44. Angajala, G.; Subashini, R. Synthesis, molecular modeling, and pharmacological evaluation of new 2-substituted benzoxazole derivatives as potent anti-inflammatory agents. *Struct. Chem.* **2020**, *31*, 263–273. [[CrossRef](#)]
45. Barcin, T.; Yucel, M.A.; Ersan, R.H.; Alagoz, M.A.; Dogen, A.; Burmaoglu, S.; Algul, O. Deep learning approach to the discovery of novel bisbenzazole derivatives for antimicrobial effect. *J. Mol. Struct.* **2024**, *1295*, 136668. [[CrossRef](#)]
46. Sattar, R.; Mukhtar, R.; Atif, M.; Hasnain, M.; Irfan, A. Synthetic transformations and biological screening of benzoxazole derivatives: A review. *J. Heterocycl. Chem.* **2020**, *57*, 2079–2107. [[CrossRef](#)]
47. Kakkar, S.; Kumar, S.; Narasimhan, B.; Lim, S.M.; Ramasamy, K.; Mani, V.; Shah, S.A.A. Design, synthesis and biological potential of heterocyclic benzoxazole scaffolds as promising antimicrobial and anticancer agents. *Chem. Cent. J.* **2018**, *12*, 96–107. [[CrossRef](#)]
48. Campo, L.F.; Rodembusch, F.S.; Stefani, V. New fluorescent monomers and polymers displaying an intramolecular proton-transfer mechanism in the electronically excited state (ESIPT). IV. Synthesis of acryloylamide and diallylamino benzazole dyes and its copolymerization with MMA. *J. Appl. Polym. Sci.* **2006**, *99*, 2109–2116. [[CrossRef](#)]
49. Park, S.; Kim, S.; Seo, J.; Park, S.Y. Application of excited-state intramolecular proton transfer (ESIPT) principle to functional polymeric materials. *Macromol. Res.* **2008**, *16*, 385–395. [[CrossRef](#)]
50. Wakita, J.; Inoue, S.; Kawanishi, N.; Ando, S. Excited-state intramolecular proton transfer in imide compounds and its application to control the emission colors of highly fluorescent polyimides. *Macromolecules* **2010**, *43*, 3594–3605. [[CrossRef](#)]
51. Liang, N.; Kuwata, S.; Ishige, R.; Ando, S. Large-Stokes-shifted yellow photoluminescence emission from an imide and polyimides forming multiple intramolecular hydrogen bonds. *Mater. Chem. Front.* **2022**, *6*, 24–32. [[CrossRef](#)]
52. Berbigier, J.F.; Duarte, L.G.T.A.; Perez, J.M.; Mendes, R.A.; Zapp, E.; Atvars, T.D.Z.; Dal-Bó, A.G.; Rodembusch, F.S. Excited state intramolecular proton transfer process in benzazole fluorophores tailored by polymeric matrix: A combined theoretical and experimental study. *J. Mol. Liq.* **2019**, *295*, 111710. [[CrossRef](#)]
53. Hwang, S.H.; Kim, H.; Ryu, H.; Serdiuk, I.E.; Lee, D.; Choi, T.L. Powerful direct C–H amidation polymerization affords single-fluorophore-based white-light-emitting polysulfonamides by fine-tuning hydrogen bonds. *J. Am. Chem. Soc.* **2022**, *144*, 1778–1785. [[CrossRef](#)] [[PubMed](#)]

54. Chen, C.L.; Chen, Y.T.; Demchenko, A.P.; Chou, P.T. Amino proton donors in excited-state intramolecular proton-transfer reactions. *Nat. Rev. Chem.* **2018**, *2*, 131–143. [[CrossRef](#)]
55. Kirkbright, G.F.; Spillane, D.E.M.; Anthony, K.; Brown, R.G.; Hepworth, J.D.; Hodgson, K.W.; West, M.A. Determination of the fluorescence quantum yields of some 2-substituted benzothiazoles. *Anal. Chem.* **1984**, *56*, 1644–1647. [[CrossRef](#)]
56. Anthony, K.; Brown, R.G.; Hepworth, J.D.; Hodgson, K.W.; May, B.; West, M.A. Solid-state fluorescent photophysics of some 2-substituted benzothiazoles. *J. Chem. Soc. Perkin Trans. 2* **1984**, 2111–2117. [[CrossRef](#)]
57. Rodembusch, F.S.; Leusin, F.P.; Medina, L.F.C.; Brandelli, A.; Stefani, V. Synthesis and spectroscopic characterization of new ESIPT fluorescent protein probes. *Photochem. Photobiol. Sci.* **2005**, *4*, 254–259. [[CrossRef](#)] [[PubMed](#)]
58. Holler, M.G.; Campo, L.F.; Brandelli, A.; Stefani, V. Synthesis and spectroscopic characterisation of 2-(2'-hydroxyphenyl)benzazole isothiocyanates as new fluorescent probes for proteins. *J. Photochem. Photobiol. A Chem.* **2002**, *149*, 217–225. [[CrossRef](#)]
59. Barni, E.; Savarino, P.; Marzona, M.; Piva, M. 2-(4-Alkylamido-2-hydroxyphenyl) benz-X-azoles as intermediates for the synthesis of dyes. *J. Heterocyclic. Chem.* **1983**, *20*, 1517–1521. [[CrossRef](#)]
60. Orlandini, L.F.; Rodembusch, F.S.; De Luca, M.A.; Jacobi, M.A.M.; Stefani, V. New fluorescent elastomeric materials based on synthetic and natural epoxidized rubbers. *J. Appl. Polym. Sci.* **2008**, *109*, 282–287. [[CrossRef](#)]
61. Isoppo, V.G.; Rodrigues, M.O.; Rodembusch, F.S.; Moro, A.V. 2,1,3-Benzothiadiazole-based bis-silylated compounds: Synthesis and use in the preparation of highly fluorescent low-content organic-inorganic hybrid materials. *J. Photochem. Photobiol. A Chem.* **2023**, *435*, 114277. [[CrossRef](#)]
62. Chi, H.; Xu, K.; Wu, X.; Chen, Q.; Xue, D.; Song, C.; Zhang, W.; Wang, P. Effect of acetylation on the properties of corn starch. *Food Chem.* **2008**, *106*, 923–928. [[CrossRef](#)]
63. Diop, C.I.K.; Li, H.L.; Xie, B.J.; Shi, J. Effects of acetic acid/acetic anhydride ratios on the properties of corn starch acetates. *Food Chem.* **2011**, *126*, 1662–1669. [[CrossRef](#)] [[PubMed](#)]
64. Zhang, L.; Xie, W.; Zhao, X.; Liu, Y.; Gao, W. Study on the morphology, crystalline structure and thermal properties of yellow ginger starch acetates with different degrees of substitution. *Thermochim. Acta* **2009**, *495*, 57–62. [[CrossRef](#)]
65. van Soest, J.J.G.; Vliegthart, J.F.G. Crystallinity in starch plastics: Consequences for material properties. *Trends Biotechnol.* **1997**, *15*, 208–213. [[CrossRef](#)] [[PubMed](#)]
66. Bogracheva, T.Y.; Wang, Y.L.; Wang, T.L.; Hedley, C.L. Structural studies of starches with different water contents. *Biopolymers* **2002**, *64*, 268–281. [[CrossRef](#)] [[PubMed](#)]
67. Bogracheva, T.Y.; Meares, C.; Hedley, C.L. The effect of heating on the thermodynamic characteristics of potato starch. *Carbohydr. Polym.* **2006**, *63*, 323–330. [[CrossRef](#)]
68. Cooke, D.; Gidley, M.J. Loss of crystalline and molecular order during starch gelatinisation: Origin of the enthalpic transition. *Carbohydr. Res.* **1992**, *227*, 103–112. [[CrossRef](#)]
69. Elomaa, M.; Asplund, T.; Soininen, P.; Laatikainen, P.; Peltonen, S.; Hyvarinen, S.; Urtti, A. Determination of the degree of substitution of acetylated starch by hydrolysis, ¹H NMR and TGA/IR. *Carbohydr. Polym.* **2004**, *57*, 261–267. [[CrossRef](#)]
70. Shi, R.; Bi, J.; Zhang, Z.; Zhu, A.; Chen, D.; Zhou, X.; Zhang, L.; Tian, W. The effect of citric acid on the structural properties and cytotoxicity of the polyvinyl alcohol/starch films when molding at high temperature. *Carbohydr. Polym.* **2008**, *74*, 763–770. [[CrossRef](#)]
71. Becker, M.R.; Stefani, V.; Forte, M.M.C. Novel fluorescent copolymers of styrene with benzazole chromophores. *React. Funct. Polym.* **2001**, *66*, 1664–1669. [[CrossRef](#)]
72. Xin, J.Y.; Wang, Y.; Liu, T.; Lin, K.; Chang, L.; Xia, C.G. Biosynthesis of corn starch palmitate by lipase Novozym 435. *Int. J. Mol. Sci.* **2012**, *13*, 7226–7236. [[CrossRef](#)] [[PubMed](#)]
73. Bertolini, A.C.; Mestres, C.; Raffi, J.; Buléon, A.; Lerner, D.; Colonna, P. Photodegradation of cassava and corn starches. *J. Agric. Food Chem.* **2001**, *49*, 675–682. [[CrossRef](#)] [[PubMed](#)]
74. Berbigier, J.F.; Duarte, L.G.T.A.; Zawacki, M.; de Araújo, B.; Santos, C.; Atvars, T.D.Z.; Gonçalves, P.F.B.; Petzhold, C.L.; Rodembusch, F.S. ATRP initiators based on proton transfer benzazole dyes: Solid state photoactive polymer with very large Stokes shift. *ACS Appl. Polym. Mater.* **2020**, *2*, 1406–1416. [[CrossRef](#)]
75. Rodembusch, F.S.; Campo, L.F.; Stefani, V.; Rigacci, A. The first silica aerogels fluorescent by excited state intramolecular proton transfer mechanism (ESIPT). *J. Mater. Chem.* **2005**, *15*, 1537–1541. [[CrossRef](#)]
76. Chung, K.Y.; Chen, Y.H.; Chen, Y.T.; Hsu, Y.H.; Shen, J.Y.; Chen, C.L.; Chen, Y.A.; Chou, P.T. The excited-state triple proton transfer reaction of 2,6-diazaindoles and 2,6-diazatryptophan in aqueous solution. *J. Am. Chem. Soc.* **2017**, *139*, 6396–6402. [[CrossRef](#)]
77. Lochbrunner, S.; Wurzer, A.J.; Riedle, E. Microscopic mechanism of ultrafast excited-state intramolecular proton transfer: A 30-fs study of 2-(2'-hydroxyphenyl)benzothiazole. *J. Phys. Chem. A* **2003**, *107*, 10580–10590. [[CrossRef](#)]

Disclaimer/Publisher's Note: The statements, opinions and data contained in all publications are solely those of the individual author(s) and contributor(s) and not of MDPI and/or the editor(s). MDPI and/or the editor(s) disclaim responsibility for any injury to people or property resulting from any ideas, methods, instructions or products referred to in the content.